ELSEVIER

Journal of Molecular Catalysis A: Chemical 136 (1998) 185–194

JOURNAL OF MOLECULAR CATALYSIS A: CHEMICAL

Dissociation of methane on different transition metals

Meng-Sheng Liao *, Qian-Er Zhang

State Key Laboratory for Physical Chemistry of Solid Surfaces, Chemistry Department, Xiamen University, Xiamen 361005, China

Received 24 November 1997; accepted 16 January 1998

Abstract

Dissociation of methane on different transition metals M (M = Ru, Ir, Rh, Ni, Pd, Pt, Cu, Ag, Au) has been investigated using a quasi-relativistic density-functional method. Reaction enthalpies for the steps involved are determined. The activation energies have been estimated using the analytic BOC-MP formula. The transition metals, Ru, Rh, ..., Pt are shown to exhibit high activity in the dissociation of methane, whereas the coinage metals (Cu, Ag, Au) are very inactive. The conclusion is in agreement with experimental observations. The total dissociation enthalpy ΔH for the complete dissociation of CH_4 to give surface C and H ($CH_{4,s} \rightarrow C_s + 4H_s$) can be regarded as a measure for the activity of the metal in methane dissociation. The order of the calculated ΔH's is consistent with the order of methane conversions over the metals. The dissociation of methane is also examined in the presence of adsorbed oxygen. Oxygen at on-top site promotes methane dehydrogenation. Oxygen at hollow site promotes methane dehydrogenation on Pt and the coinage metals, but is not beneficial to that on the other transition metals.

Keywords: Methane dissociation; Transition metals; Density-functional calculations

1. Introduction

The conversion of methane to higher hydrocarbons constitutes an active subject for catalytic research. Various processes have been proposed. A possible route is the oxidative coupling of methane (OCM) reaction to produce C_2 hydrocarbons. Basic oxides such as rare earth oxides, alkaline earth oxides and alkali metal-doped metal oxides are known to be active and selective catalysts in the OCM reaction [1]. Up to now, however, only indirect routes via syngas (CO, H_2) formation have been commercialized to utilize methane. Syngas is produced from methane mostly by steam reforming ($CH_4 + H_2O \rightarrow CO + 3H_2$), which suffers from disadvantage of high energy requirement, high H_2/CO_2 ratio (> 4, which is not suitable for methanol and Fischer–Tropsch synthesis) and poor selectivity for CO. The catalytic oxidation of methane to syngas (we denote it as OMS)

$$CH_4 + \tfrac{1}{2}O_2 \rightarrow CO + H_2 \qquad (1a)$$

has been suggested as promising alternative route. The OMS reaction is mildly exothermic, more selective and produces more desirable H_2/CO ratio. Recently, a series of supported nickel and noble metal catalysts were found to be active in OMS [2–22].

Two different mechanisms for the catalytic OMS process have been proposed in the litera-

* Corresponding author.

1381-1169/98/$ - see front matter
PII: S1381-1169(98)00050-8

ture. Since the early work of Prettre et al. [23], it has been accepted that the reaction process involves first the oxidation of CH_4 primarily to H_2O and CO_2 followed by the steam reforming reaction of CH_4 with H_2O and the water-gas shift reaction. Various data have been advanced in support of this opinion [2–7]. The other mechanism is direct oxidation via methane pyrolysis as proposed by Schmidt et al. [8–12] based on experiments over monolith-supported Rh and Pt catalysts at short contact time. According to the latter authors, the dissociation of methane is an initial step; H_2 and CO are formed via surface species (CH_x, H) originated from the methane dissociation. The latter mechanism has been supported by a series of recent pulse studies of OMS [13–22]. It was also concluded [16–18] that CH_4 conversion depends on its dissociation.

Since the catalytic OMS process is rather complex, the experimental conditions adopted may strongly influence the reaction steps. From the various studies [2–23], one may conclude that the contact time between reactant and catalyst is an important factor that can affect the reaction scheme, as claimed by Schmidt et al. [11,12]. It is, therefore, expected that shortening of the residence time can give direct catalytic OMS. The objective of this paper is to present a theoretical investigation of dissociation of methane on a number of transition metals M (M = Ru, Rh, Ir, Ni, Pd, Pt, Cu, Ag and Au), thereby extending the previous work [24]. An experimental comparative study by Schmidt et al. [11,12] has shown that the Ni and Rh catalysts exhibit higher activity in the OMS than other metal catalysts. Coinage metals (Cu, Ag, Au) are known to be far less active in the OMS [20,21]. To understand the chemistry of methane on these materials, the study of dissociation of methane on single-crystal surfaces would be a key step. According to pulse studies [16–22], reduced catalysts activate CH_4 much more easily than metal oxides. It was therefore concluded that reduced metals are the main active site for syngas formation.

The paper is organized as follows. Computational method and models are given in Section 2. The adsorption properties of intermediate fragments (CH_x, H, O, OH), the dissociation of methane on the metal surfaces, and oxygen-assisted dissociation are discussed in Section 3. Our conclusions are summarized in Section 4.

2. Computational method and metal surface modelling

The quantum chemical calculations reported in this paper were performed using the Amsterdam Density Functional (ADF) program package developed by Baerends et al. [25,26]. The frozen core approximation [25,26] was used here to reduce the computational cost. For C and O, the 1s shell was frozen. For the metal atoms, the electrons up to and including $(n-1)$p shells were kept frozen. The valence shells, i.e., $(n-1)$d $-$ ns for the metal atoms, 2s $-$ 2p for C and O, 1s for H are expanded in triple-zeta STO basis sets extended by single-zeta STO sets for the inner core wiggles and by single-zeta polarization function (np for the metals, 3d for C and O, 2p for H). The exchange-correlation potential used was based on the density-parameterized form of Vosko, Wilk and Nusair (VWN) [27]. The non-local corrections used were based on Becke's gradient functional for exchange [28] and Perdew's gradient functional for correlation [29]. These corrections are included in a self-consistent manner. Relativistic corrections of the valence electrons were calculated using the quasi-relativistic method due to Ziegler et al. [30].

We choose metal M(111) as the surface for adsorption. M(111) is simulated by a two-layer-thick M_{10} cluster which contains seven metal atoms in the first layer and three metal atoms in the second for an on-top site model (M(7,3)), and vice versa (M(3,7)) for a hollow site model. In practice, only a smaller Ni_7 cluster was used for Ni(111) because we had the SCF convergence problem with the larger Ni_{10}

cluster. A M_7 cluster model contains one metal atom in the first layer and six metal atoms in the second (M(1,6)) for an on-top site model and vice versa (M(6,1)) for a hollow site model. Therefore we have also presented here the calculated results on Pd_7 and Pt_7 so that the results on Ni(111) could be compared adequately with those on Pd(111) and Pt(111) within a same group. Furthermore, a larger M_{13} cluster, where M(7,6) is for an on-top site model and M(6,7) is for a hollow site model, was also tested for M = Pd and Cu in order to examine the influence of cluster size on the calculated results.

The geometries for the CH_x ($x = 4, \ldots, 1$) and OH species adsorbed on the metal surfaces are shown in Fig. 1. The molecular parts above the surface were fully optimized under the constraint of the symmetries given in the figure. The O–H bond is found to be perpendicular to the metal surface. The M–M distances are taken from the experimental values for the bulk crystals and kept frozen during the model calculations.

According to the pulse studies [16–18,22], there were at least two possible pathways for

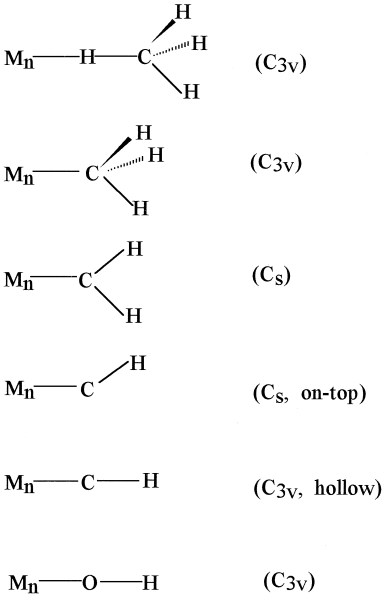

Fig. 1. Geometries of the CH_x ($x = 4, \ldots, 1$) and OH species adsorbed on the metal M_n cluster.

methane dissociation, viz. direct dissociation and oxygen-assisted dissociation. Our calculations considered two types of adsorbed oxygen species (O_s) located at on-top and hollow sites, which represent the 'weakly' and 'strongly' adsorbed oxygen, respectively.

3. Results and discussion

3.1. Adsorption energies of intermediate fragments (CH_x, H, O)

Methane decomposition on 'reduced transition metals' results in CH_x ($x = 3, 2, 1, 0$) and H species. So the adsorption energies of the various species play an essential role in the methane dissociation. The results are collected in Table 1, together with available experimental data. The preferred sites for the various species have been identified. At present, only two sites, on-top and threefold hollow, are considered. Table 2 gives the calculated heights of the species above the metal surfaces. Table 3 shows the Mulliken charge distributions on the whole adsorbed species.

Let us first examine the cluster size effect. For M = Pd, three cluster sizes Pd_7, Pd_{10} and Pd_{13} are investigated here. We see that there is no significant variation of the calculated adsorption energies with cluster size. For M = Pt, the results on Pt_7 are also quite close to those on Pt_{10}. Therefore, one may conclude that the cluster size effect on the calculated adsorption energies is small for the platinum group. For the coinage metal Cu, the M_{10} and M_{13} clusters give also similar results.

3.1.1. Adsorbed CH_4

The CH_4 bond to the metal surface is very weak. This is to be expected since CH_4 is very stable saturated molecule. The on-top site of the metal surface is found to be slightly more favorable than the hollow site for the CH_4 adsorption. The M–H distances are generally large,

Table 1
Calculated adsorption energies[a] E (eV) for various species adsorbed on M_n cluster model of M(111) (t = top, h = hollow) Experimental data, which are indicated in italics here, are those cited in Ref. [31]

	Ru_{10}	Rh_{10}	Ir_{10}	Ni_7	Pd_{10}	Pt_{10}	Cu_{10}	Ag_{10}	Au_{10}
CH_4(t)	0.03	0.03	0.12	0.09	0.04	0.14	0.02	0.01	0.02
					0.08[b]	0.18[b]			
					0.04[c]		0.01[c]		
CH_3	2.00(h)	1.87(h)	1.76(t)	1.94(t)	1.54(t)	1.77(t)	1.15(h)	0.47(t)	0.75(t)
					1.31(t)	1.75(t)			
					1.66(t)		1.28(h)		
CH_2(h)	4.26	4.37	4.33	3.92	3.21	3.66	3.01	1.87	2.15
					3.54	3.48			
					3.28		2.75		
CH(h)	6.81	7.14	7.21	7.14	5.74	6.71	4.50	3.02	4.19
					6.26	6.27			
					6.19		4.51		
C(h)	7.37	7.77	7.63	7.65	6.67	7.40	3.73	2.27	3.39
					6.37	6.75			
					6.82		3.89		
				7.42					
H	2.82(h)	2.89(h)	2.71(t)	2.97(h)	2.64(h)	2.59(h)	2.12(h)	1.63(h)	1.81(h)
						2.94(h)	2.84(h)		
						2.70(h)		2.28(h)	
	2.91	*2.65*	*2.52*	*2.73*	*2.69*	*2.65*	*2.43*	*< 2.47*	*< 2.52*
O(t)	4.42	3.64	3.13	4.79	3.15	2.71	2.28	1.66	0.89
O(h)	6.24	6.67	5.62	5.59	4.09	4.24	5.07	3.60	3.12
	4.34	*4.42*	*4.03*	*4.99*	*3.77*	*3.69*	*4.77*	*3.47*	*< 3.25*
H → O[d](t)	2.88	2.94	3.17	3.66	3.32	3.34	4.49	4.75	4.68
					4.19	3.44			
					3.45		4.21		
H → O[d](h)	2.74	2.57	2.58	1.76	2.51	2.91	2.67	3.51	3.18
					2.39	2.84			
					2.20		3.12		

[a] For the CH_x ($x = 4, \ldots, 0$) H species, only the results calculated at preferred site are given.
[b,c] Values in the second and third rows are results calculated on the M_7 and M_{13} clusters, respectively; the same is true for the other species.
[d] Represents adsorption of H on surface O.

Table 2
Calculated heights[a] (in Å) above the metal surface (t = top, h = hollow)

	Ru_{10}	Rh_{10}	Ir_{10}	Ni_7	Pd_{10}	Pt_{10}	Cu_{10}	Ag_{10}	Au_{10}
CH_4(t)	2.20	2.19	2.02	2.29	2.10	2.05	2.29	2.70	2.30
CH_3	1.61(h)	1.70(h)	2.05(t)	1.91(t)	2.04(t)	2.08(t)	1.65(h)	2.26(t)	2.16(t)
CH_2(h)	1.50	1.41	1.53	1.23	1.35	1.36	1.40	1.55	1.49
CH(h)	1.24	1.15	1.16	1.06	1.09	1.18	1.19	1.57	1.16
C(h)	1.22	1.11	1.19	1.00	1.03	1.05	1.18	1.37	0.98
H	1.04(h)	0.95(h)	1.64(t)	0.81(h)	0.78(h)	0.79(h)	0.94(h)	0.93(h)	0.82(h)
O(t)	1.71	1.72	1.75	1.61	1.87	1.87	1.80	2.07	2.05
O(h)	1.26	1.16	1.26	1.05	1.20	1.21	1.22	1.40	1.40
HO(t)	1.90	1.92	1.91	1.73	2.07	2.08	1.94	2.19	2.28
HO(h)	1.56	1.62	1.70	1.40	1.62	1.65	1.46	1.75	1.73

[a] The heights calculated on the different cluster sizes are very similar, and so the values on Pd_7, Pd_{13}, Pt_7 and Cu_{13} are not listed here.

Table 3
Mulliken charge distributions (in e) on the whole adsorbed species (t = top, h = hollow)

	Ru_{10}	Rh_{10}	Ir_{10}	Ni_7	Pd_{10}	Pt_{10}	Cu_{10}	Ag_{10}	Au_{10}
CH_4(t)	0.12	0.10	−0.09	0.05	0.15	−0.08	0.18	0.10	0.09
					0.05[a]	−0.17[a]			
					0.16[b]		0.19[b]		
CH_3	−0.75(h)	−0.47(h)	−0.19(t)	−0.14(t)	−0.32(t)	−0.14(t)	−0.02((h)	−0.17(t)	−0.27(t)
					−0.42(t)	−0.60(t)			
					−0.28(t)		0.08(h)		
CH_2(h)	−0.88	−0.84	−1.12	−0.17	−1.02	−1.32	−0.46	−0.67	−1.41
					−0.98	−1.36			
					−1.00		−0.25		
CH(h)	−1.18	−1.11	−1.78	−0.38	−1.27	−1.72	−0.79	−1.19	−2.10
					−1.24	−1.91			
					−1.29		−0.57		
C(h)	−0.80	−0.79	−1.06	−0.31	−0.93	−1.30	−0.51	−0.65	−1.88
					−0.92	−1.26			
					−1.08		−0.32		
H	−0.42(h)	−0.38(h)	−0.19(t)	−0.02(h)	−0.85(h)	−0.89(h)	−0.07(h)	−0.33(h)	−0.98(h)
					−0.69(h)	−0.77(h)			
					−0.93(h)		0.00(h)		
O(t)	−0.51	−0.54	−0.51	−0.64	−0.54	−0.54	−0.65	−0.69	−0.58
O(h)	−0.92	−0.90	−0.94	−0.64	−0.87	−0.98	−0.82	−0.83	−0.86
HO(t)	−0.39	−0.44	−0.44	−0.36	−0.44	−0.44	−0.45	−0.56	−0.46
					−0.48	−0.58			
					−0.46		−0.42		
HO(h)	−0.56	−0.46	−0.44	−0.30	−0.56	−0.48	−0.43	−0.51	−0.49
					−0.39	−0.28			
					−0.56		−0.37		

[a,b] Values in the second and third rows are results calculated on the M_7 and M_{13} clusters, respectively; the same is true for the other species.

especially the Ag–H one. The Ir–H and Pt–H distances are relatively small. So there are also relatively large M–H bond strengths. It is interesting to find that the M–H distance decreases in the order Ni–H > Pd–H > Pt–H. The Rh–H distance is also significantly larger than the Ir–H one. Due to the close approach, there is a little charge transfer (0.1 e) from Ir_{10} or Pt_{10} to CH_4. On the other metals, the Mulliken charge on the whole CH_4 species are positive, indicating charge transfer from the adsorbate to the cluster.

3.1.2. Adsorbed CH_3

CH_3 can adsorb rather strongly on the metal surfaces. The bonding sites are not same for the different metals. On Ru, Rh and Cu, the hollow site is preferred, while the on-top site is preferred on the other metals for adsorbed CH_3. It is found that the energy difference (Δ) between the sites is rather small on Rh ($\Delta = 0.14$ eV) and Ag ($\Delta = 0.06$ eV). With use of a larger Ag_{13} cluster, the hollow site is calculated to be slightly more favorable than the on-top site ($\Delta = 0.10$ eV). Because of some uncertainties in the calculated results, the differences in energy may be too small for one to make a definite assignment of the bonding site on the two metals. Our calculated adsorption energy of 1.94 eV on Ni is quite close to the accurate contracted CI value of 2.0–2.2 eV calculated using varying cluster model and so-called 'bond-prepared' states [32]. The adsorption energies on metals in a same group vary in the order: Ni > Pt > Pd and Cu > Au > Ag. The adsorption energies on the coinage metals are significantly smaller than those on the other transition metals.

3.1.3. Adsorbed CH_2, CH and C

For the adsorptions of these species, the hollow site is clearly preferred. There are major differences in the adsorption energies of these species at the different sites. The argument [33] is that C in the un-saturated CH_x species has a tendency to restore its missing bond. Hence the energy difference $\Delta^{top-hol}$ for CH or C is found to be much more pronounced than for CH_2. The only experimental adsorption energy is for C on Ni. The calculated and experimental values are in very good agreement. For the transition metals, Ru–Pt, the adsorption energy E_{ads} of CH_x increases on going from $x = 3$ to $x = 0$. There is a strong increase in E_{ads} from $x = 3$ to $x = 1$. In contrast, the difference between the metal–CH and metal–C bond strengths is relatively small. For the coinage metals, there is an abnormal order of E_{ads}'s: $CH_2 < CH$. The charge transfer from the metal to the CH_x group is significant. The negative charge ΣQ on CH_x increases from Ni to Pt and from Cu to Au, indicating a decrease in the surface electronegativity from the top to bottom of a column.

3.1.4. Adsorbed H and O

H favors the hollow site on the metals. Ir is the only exception, where atomic H is more strongly bound at the on-top site than at the hollow site. Unlike C, experimental values of the adsorption energy of H are known for many metals. All the calculated values are close to the experimentally measured ones, the error typically not exceeding 0.3 eV. For M = Ag and Au, experimental studies suggested that the values are < 2.5 eV. The calculated results are about 1.8 eV, in agreement with the experimental predictions. The calculations also show that adsorption energies of H on coinage metals are significantly smaller than those on the other transition metals. A notable fact is that the values of the adsorption energy of H are much smaller than the energy required for the breakage of the tetrahedral CH bond (4.85 eV^{calc}, 4.51 eV^{exp}). Hence the generation of gas-phase CH_3 via H-abstraction from CH_4 is difficult on the metal surfaces. This is the reason why CH_4 activated by metal surfaces is selectively oxidized to syngas, rather than higher carbon products.

For adsorption of O on M(111), the better location is also at the hollow site, similar to the C and H cases. The BOC-MP model [31] predicts that high-coordination site is always preferred for atoms. Our calculations provide an evidence for this conclusion. On the coinage metals, the adsorption energies E_{ads} of O are larger or comparable (for M = Au) than those of C. On the other transition metals, the E_{ads} values of O are considerably smaller than those of C. Compared with the experimental data, the calculated values (at the preferred site) are all too large, by 0.1–2.2 eV, depending on the metal. The net charge of O at the hollow site is higher than at the on-top site.

The adsorption of H on surface oxygen O_s results in the formation of OH_s. The surface-O^{top} distances are then expanded by 0.15–0.2 Å. The expansion of surface-O^{hol} is much more pronounced, by 0.3–0.4 Å. The calculated adsorption energies of H on O^{top} are larger than those on O^{hol}, by 0.2–2 eV, depending on the metal. Compared to the bare metal surfaces, the presence of O^{top} increases the adsorption energy of H, but the magnitude of the increase in E_{ads} is different for the different metal. The presence of surface-O^{hol} increases the adsorption energies of H on Pt and on all coinage metals, but plays an opposite role on the other metals.

3.2. Dissociation of methane

The dissociation of methane on the metal surface involves a sequential dehydrogenation of CH_4 (s = surface)

$$CH_{x,s} \rightarrow CH_{x-1,s} + H_s \quad (x = 4,3,2,1) \qquad (1b)$$

Because it is difficult to determine transition states for the reactions on metal surface, we focus mainly on an evaluation of the reaction enthalpies ΔH_s which should be one of the important factors that determine the OMS pro-

cess. The calculated adsorption energies given in Table 1 together with the calculated C–H bond strengths in the gas-phase $CH_{x,g}$ can be used to determine ΔH_s. The scheme is shown as follows:

$$\begin{array}{lll} CH_{x,s} \overset{\Delta H_s}{\rightarrow} & CH_{x-1,s} + & H_s \\ \uparrow -E_1 & \uparrow -E_2 & \uparrow -E_H \\ CH_{x,g} \underset{\Delta H_g}{\rightarrow} & CH_{x-1,g} + & H_g \end{array} \quad (2)$$

$$\Delta H_s = \Delta H_g + E_1 - E_2 - E_H \quad (3)$$

where E_1, E_2 and E_H are the adsorption energies of CH_x, CH_{x-1} and H, respectively; the term ΔH_g represents the reaction (dissociation) enthalpy of CH_x in the gas-phase.

In order to acquire some ideas about the barrier heights, the Bond-Order Conservation Morse-Potential (BOC-MP) approach developed by Shustorovich [31] is employed here to evaluated the activation energies. This approach has proven to be efficient for treating energetics of molecular adsorbates on transition metals. The analytic BOC-MP formula relates the activation energy $E*$ to the adsorption energies of an adsorbate and its dissociative fragments on the surface. For reaction 1, the formula is given by:

$$E^* = \frac{1}{2}\left(\Delta H_g + \frac{E_2 E_H}{E_2 + E_H} + E_1 - E_2 - E_H\right) = \frac{1}{2}\left(\frac{E_2 E_H}{E_2 + E_H} + \Delta H_s\right) \quad (4)$$

Here the energy terms are shown in Scheme 2. According to Eq. (4), the BOC-MP formula also reveals a correlation between the activation energy and reaction enthalpy for reaction 1. The calculated reaction enthalpies and activation energies are given in Tables 4 and 5, respectively.

There have been many experimental studies of methane activation on Ni surfaces [34–36]. For the dissociative chemisorption of CH_4 on Ni(111), the activation energy E^* determined by Beebe et al. [35,36] is 12.6 kcal/mol (0.55 eV) and is believed to be likely accurate [37]. Our calculated value of 0.60 eV agrees well with the experimental value. Several theoretical studies of methane activation on Ni(111) with metallic clusters of finite size have been reported in the literature. The calculated activation energies are 0.66 eV [37], 0.74 eV [38], 1.25 eV [39], 0.97 eV [40], 1.04 eV [41]. The

Table 4
Calculated dissociation enthalpies ΔH_s (eV) (Scheme 2) (s = surface)

	Ru_{10}	Rh_{10}	Ir_{10}	Ni_7	Pd_{10}	Pt_{10}	Cu_{10}	Ag_{10}	Au_{10}
$CH_{4,s} \rightarrow CH_{3,s} + H_s$	0.06	0.12	0.50	0.03	0.71	0.63	1.60	2.76	2.31
					0.68[a]	0.44[a]			
					0.54[b]		1.30[b]		
$CH_{3,s} \rightarrow CH_{2,s} + H_s$	0.05	−0.26	−0.15	0.18	0.82	0.65	1.15	2.33	1.92
					−0.02	0.56			
					0.81		1.38		
$CH_{2,s} \rightarrow CH_s + H_s$	−0.44	−0.73	−0.66	−1.26	−0.24	−0.71	1.32	2.15	1.08
					−0.73	−0.70			
					−0.68		0.89		
$CH_s \rightarrow C_s + H_s$	0.34	0.20	0.59	0.24	0.15	0.44	2.37	2.84	2.71
					0.67	0.40			
					0.39		2.06		
$CH_{4,s} \rightarrow C_s + 4H_s$	0.01	−0.67	0.28	−0.81	1.44	1.01	6.44	10.08	8.02
					0.58	0.70			
					1.06		5.63		

[a,b] Values in the second and third rows are results calculated on the M_7 and M_{13} clusters, respectively; the same is true for the other reactions.

Table 5
Calculated activation energies $E*$ (eV) (Eq. (4)) (s = surface)

	Ru_{10}	Rh_{10}	Ir_{10}	Ni_7	Pd_{10}	Pt_{10}	Cu_{10}	Ag_{10}	Au_{10}
$CH_{4,s} \rightarrow CH_{3,s} + H_s$	0.62	0.63	0.79	0.60	0.84	0.84	1.12	1.54	1.42
					0.79[a]	0.76[a]			
					0.77[b]		1.01[b]		
$CH_{3,s} \rightarrow CH_{2,s} + H_s$	0.88	0.74	0.76	0.94	1.14	1.09	1.20	1.60	1.45
					0.80	1.06			
					1.15		1.31		
$CH_{2,s} \rightarrow CH_s + H_s$	0.78	0.67	0.66	0.42	0.79	0.58	1.38	1.61	1.17
					0.64	0.63			
					0.60		1.20		
$CH_s \rightarrow C_s + H_s$	1.19	1.16	1.30	1.19	1.02	1.18	1.86	1.90	1.95
					1.34	1.20			
					1.16		1.75		

[a,b] Values in the second and third rows are results calculated on the M_7 and M_{13} clusters, respectively; the same is true for the other reactions.

activation energies of CH_4 calculated on Ru and Rh are similar to that on Ni. The activation energies of CH_4 on the other metals are larger than that on Ni, by ~ 0.2 eV for M = Pd and Pt, ~ 0.5 eV for M = Cu, ~ 1 eV for M = Ag and Au. A schematic illustration of $E*(CH_4)$ calculated on the various metals is shown in Fig. 2. There is the following order of the $E*(CH_4)$ values: Ru ≈ Rh ≈ Ni < Ir ≈ Pd ≈ Pt < Cu < Ag ≈ Au.

Dehydrogenations of CH_x to $CH_{x\text{-}1}$ are highly endothermic in the gas-phase, the calculated ΔH_g values being: CH_3–H, 4.85 eV; CH_2–H, 5.13 eV; CH–H, 4.93 eV; C–H, 3.72 eV. On the metal surface, there is a significant reduction in the ΔH's, owing to the presence of strong metal-CH_{x-1} and metal-H bonds. On Ni, the first dehydrogenation step $CH_{4,s} \rightarrow CH_{3,s} + H_s$ is nearly thermoneutral. For the subsequent dehydrogenations of $CH_{x,s}$ ($x = 3,2,1$), one step is rather exothermic and two steps are slightly endothermic. On Pd and Pt, one step is mildly exothermic and three steps are mildly endothermic. On Rh, two steps are mildly exothermic and the other two steps are slightly endothermic. On the coinage metals, all steps are rather endothermic. It is clear that a smaller dissociation enthalpy corresponds to a lower activation energy.

Summation of the enthalpies for the four discrete steps gives the total dissociation enthalpies ΔH_s^{tot} for $CH_{4,s} \rightarrow C_s + 4H_s$. It should be a more realistic measure for the activity of the metal in methane dissociation. The obtained ΔH_s^{tot} values for the various metals are given in the last row of Table 4 and schematically shown in Fig. 2. The total dissociation is shown to be quite exothermic on Ni and Rh; it is slightly endothermic on Ru and Ir (by ~ 0.3 eV) and it is rather endothermic on Pd and Pt (by ~ 1 eV). This indicates that the total dissociations of methane on Ni and Rh are thermody-

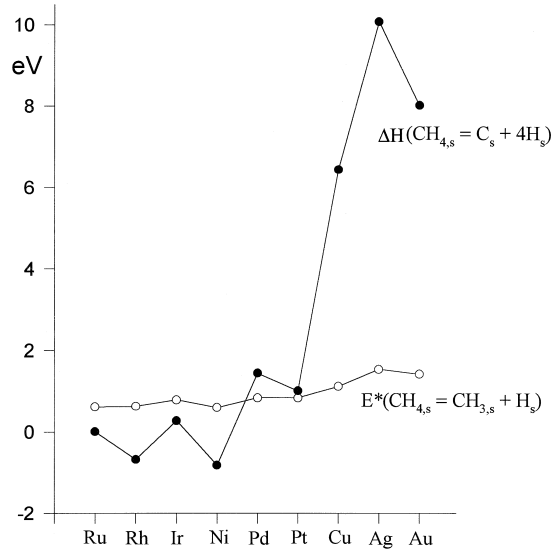

Fig. 2. Schematic illustration of calculated activation energies $E*$ ($CH_{4,s} = CH_{3,s} + H_s$) and total dissociation enthalpies for the complete dissociation of methane ($CH_{4,s} = C_s + 4H_s$).

Table 6
Difference (Δ in eV) between the dissociation enthalpies with and without the involvement of chemisorbed oxygens (s = surface)

		Δ^{top} (O at on-top)	Δ^{hol} (O at hollow)
$CH_{x,s} + O_s \rightarrow CH_{x-1,s} + OH_s$	Ru_{10}	−0.06	+0.08
	Rh_{10}	−0.05	+0.32
	Ir_{10}	−0.46	+0.13
	Ni_7	−0.69	+1.21
	Pd_{10}	−0.68	+0.13
	Pt_{10}	−0.75	−0.32
	Cu_{10}	−2.37	−0.55
	Ag_{10}	−3.12	−1.88
	Au_{10}	−2.87	−1.37

namically significantly more favorable than on the other transition metals. The ΔH_s^{tot} values vary in the order: Rh ≈ Ni < Ru < Ir < Pt < Pd. In the OMS experiments of Schmidt et al. [11,12], the methane conversions were found to be 80% on Rh and Ni, 73% on Ir, 67% on Pt, 56% on Pd. The difference in the total dissociation enthalpies is in line with the experimentally observed difference in methane conversions over the metals. We see that with use of the smaller M_7 cluster, Pd and Pt show similar ΔH_s^{tot}. This may not be thought in contradiction with the conclusion obtained. For the coinage metals, the total dissociation enthalpies are very positive, more than 5 eV (115 kcal/mol). Therefore, the coinage metals are inactive in the dissociation of methane to give surface C_s and H_s. The reaction endothermicity increases in the order Cu < Au < Ag.

3.3. Oxygen-assisted dissociation

According to the pulse studies [16–18,22], the adsorbed O species (O_s) formed in the decomposition of O_2 as well as the oxygen in metal oxide and catalyst support could participate in methane dissociation. Accordingly, in addition to the direct dissociation of methane on bare metal surface, we may consider the following reactions

$$CH_{x,s} + O_s \rightarrow CH_{x-1,s} + OH_s \quad (x = 4,3,2,1) \tag{5}$$

The methane dissociation reactions in the presence of O_s were investigated in Refs. [16–18,22] by applying the BOC-MP model, where different surface oxygens at on-top, bridge and hollow sites were examined. The BOC-MP results show that oxygen atom at on-top sites promotes methane dehydrogenation. Here we consider the adsorbed oxygens O_s at on-top and hollow sites only. The differences (Δ) between the dissociation enthalpies with and without the involvement of chemisorbed oxygens are given in Table 6.

Because the H atom binds more strongly with O_s^{top} than with bare metal, the methane dissociation reactions in the presence of O_s located at on-top sites have lower reaction enthalpies due to hydroxyl formation. This means that O_s^{top} promotes the dehydrogenation of CH_x. The calculations also show that the Δ^{top} values may be rather different for the different metals. They are in fact very small for Ru and Rh, but are large for the coinage metals. The O species at the hollow site, O_s^{hol}, shows different behavior towards the methane dissociation. O_s^{hol} increases the adsorption energies of H on Pt and the coinage metals, but decreases those on the other transition metals. Therefore, on Pt and the coinage metals, O_s^{hol} also promotes methane dissociation, but can be found to be much less strongly than O_s^{top}. On the other transition metals, O_s^{hol} is not beneficial to the methane dissociation.

4. Conclusions

In this paper, the dissociation of methane ($CH_{x,s} \rightarrow CH_{x-1,s} + H_s$, $x = 4,3,2,1$) on a

number of transition metals M has been examined (M = Ru, Rh, Ir, Ni, Pd, Pt, Cu, Ag, Au). Reaction enthalpies for the steps involved are determined and the activation energies have been estimated using the analytic BOC-MP formula. The results support that the metals from Ru to Pt are active in methane dissociation. The dissociation enthalpies are shown to be an important factor determining the catalytic activity of the metal. The order of the calculated total dissociation enthalpies ΔH ($CH_{4,s} \rightarrow C_s + 4H_s$) can be correlated to the order of methane conversions over the metals. According to the trend in the calculated ΔH's, the most efficient catalysts for methane dissociation are Rh and Ni, and the Ru and Ir metals are more active than Pd and Pt. The total dissociations of methane on the coinage metals (Cu, Ag, Au) are found to be very endothermic. Therefore, the coinage metal catalysts do not mediate methane dissociation, in agreement with experiment facts. Ag is the most inactive catalyst among the coinage metals.

In the presence of adsorbed oxygens, oxygen located at metal on-top site promotes methane dissociation; oxygen located at hollow site promotes methane dissociation on Pt and coinage metals, but exerts the opposite effect to that on the other transition metals.

Acknowledgements

This work was financially supported by the Natural Science Foundation of Fujian Province, P.R. China.

References

[1] Y. Amenomiya, V.I. Birss, M. Goledzinowski, J. Galuska, A.R. Sanger, Catal. Rev. Sci. Eng. 32 (1990) 163.
[2] P.D.F. Vernon, M.L.H. Green, A.K. Cheetham, A.T. Ashcroft, Catal. Lett. 6 (1990) 181.
[3] P.D.F. Vernon, M.L.H. Green, A.K. Cheetham, A.T. Ashcroft, Catal. Today 13 (1992) 417.
[4] D. Dissanayyake, M.P. Rosynek, K.C.C. Kharas, J.H. Lunsford, J. Catal. 132 (1991) 117.
[5] Y. Boucouvalas, Z.L. Zhang, X.E. Verykios, Catal. Lett. 27 (1994) 131.
[6] V.A. Tsipouriari, A.M. Efstathiou, Z.L. Zhang, X.E. Verykios, Catal. Today 21 (1994) 579.
[7] Z.L. Zhang, X.E. Verykios, J. Chem. Soc., Chem. Commun. (1995) p. 71.
[8] D.A. Hickman, L.D. Schmidt, J. Catal. 138 (1992) 267.
[9] D.A. Hickman, L.D. Schmidt, Science 259 (1993) 343.
[10] D.A. Hickman, E.A. Haupfer, L.D. Schmidt, Catal. Lett. 17 (1993) 223.
[11] P.M. Torniainen, X. Chu, L.D. Schmidt, J. Catal. 146 (1994) 1.
[12] S.S. Bharadwaj, L.D. Schmidt, J. Catal. 146 (1994) 11.
[13] E.P.J. Mallens, J.H.B.J. Hoebink, G.B. Marin, Catal. Lett. 33 (1995) 291.
[14] O.V. Buyevskaya, D. Wolf, M. Baerns, Catal. Lett. 29 (1994) 249.
[15] K. Walter, O.V. Buyevskaya, D. Wolf, M. Baerns, Catal. Lett. 29 (1994) 261.
[16] Y.H. Hu, E. Ruckenstein, J. Catal. 158 (1996) 260.
[17] Y.H. Hu, E. Ruckenstein, Catal. Lett. 35 (1995) 265.
[18] E. Ruckenstein, Y.H. Hu, Catal. Lett. 34 (1995) 41.
[19] C.T. Au, Y.H. Hu, H.L. Wan, Catal. Lett. 27 (1994) 199.
[20] C.T. Au, Y.H. Hu, H.L. Wan, Catal. Lett. 36 (1996) 159.
[21] C.T. Au, H.Y. Wang, H.L. Wan, J. Catal. 158 (1996) 343.
[22] C.T. Au, H.Y. Wang, J. Catal. 167 (1997) 337.
[23] M. Prettre, C. Eichner, M. Perrin, J. Chem. Soc. Faraday Trans. 43 (1946) 335.
[24] M.S. Liao, C.T. Au, C.F. Ng, Chem. Phys. Lett. 272 (1997) 445.
[25] E.J. Baerends, D.E. Ellis, P. Ros, Chem. Phys. 2 (1973) 41, ADF program package, version 2.0.1.
[26] G. te Velde, E.J. Baerends, J. Comp. Phys. 99 (1992) 84.
[27] S.H. Vosko, L. Wilk, M. Nusair, Can. J. Phys. 58 (1980) 1200.
[28] A.D. Becke, Phys. Rev. A 38 (1988) 3098.
[29] J.P. Perdew, Phys. Rev. B 33 (1986) 8822.
[30] T. Ziegler, V. Tschinke, E.J. Baerends, J.G. Snijders, W. Ravenek, J. Phys. Chem. 93 (1989) 3050.
[31] E.J. Shustorovich, Adv. Catal. 37 (1990) 101.
[32] J. Schüle, P. Siegbahn, U. Wahlgren, J. Chem. Phys. 89 (1988) 6982.
[33] C. Zheng, Y. Apeloig, R. Hoffmann, J. Am. Chem. Soc. 110 (1988) 749.
[34] R.A. Campbell, J. Szanyi, P. Lenz, D.W. Goodman, Catal. Lett. 17 (1993) 39, and references cited therein.
[35] T.P. Beebe Jr., D.W. Goodman, B.D. Kay, Chem. J. Phys. 87 (1987) 2305.
[36] T.P. Beebe Jr, D.W. Goodman, B.D. Kay, J.T. Yates Jr., J. Chem. Phys. 87 (1987) 87.
[37] A.B. Anderson, J.J. Maloney, J. Phys. Chem. 92 (1988) 809.
[38] H. Yang, J.L. Whitten, J. Chem. Phys. 96 (1992) 5529.
[39] H. Burghgraef, A.P.J. Jansen, R.A. van Santen, J. Chem. Phys. 101 (1994) 11012.
[40] A.P.J. Jansen, H. Burghgraef, Surf. Sci. 344 (1995) 149.
[41] P. Kratzer, B. Hammer, J.K. Nørskov, J. Chem. Phys. 105 (1996) 5595.